Basic Principles of Direct-Drive Ignition Target Design

Introduction

Inertial confinement fusion (ICF) is an approach to fusion that relies on the inertia of the fuel mass to provide confinement. The confined fuel must reach a high temperature and density to produce enough $D + T \longrightarrow \alpha(3.5\ \text{MeV}) + n(14.1\ \text{MeV})$ reactions so that the total energy released is much larger than the driver energy required to compress the fuel. The capsule in an ICF implosion, which is a spherical cryogenic deuterium–tritium (DT) shell filled with DT vapor, is irradiated directly by laser beams (direct-drive approach) or by x rays emitted by a high-Z enclosure (hohlraum) surrounding the target (indirect drive).[1] Only a small portion of the fuel is heated to ignition conditions in a typical ignition target. This part of the fuel forms a hot spot that initiates a burn wave that ignites the remaining fuel. In the direct-drive approach, the following stages of an implosion can be identified: At the beginning of the laser pulse, the outer portion of the pellet heats up and expands outward, creating a plasma atmosphere around the pellet. Then a critical electron density $n_{\text{cr}} = \pi mc^2/e^2\lambda_L^2$ is established outside the cold portion of the shell, where m is the electron mass, c is the speed of light, e is the electron charge, and λ_L is the laser wavelength. The laser energy is absorbed in a narrow region near the critical surface via the inverse bremsstrahlung, and the absorbed energy is transported, mainly by electrons, toward the colder portion of the shell. The cold material, heated by the thermal conduction, expands outward. Such an expansion creates an ablation pressure that, similar to the rocket effect, compresses the pellet. At the beginning of implosion, the ablation pressure launches a shock wave that propagates ahead of the thermal ablation front and increases the fuel entropy. Then, as the first shock breaks out at the rear surface of the shell, the transmitted shock is formed. It converges through the vapor to the capsule center. After reflection from the center, the shock moves outward and interacts with the incoming shell. At this point, the velocity of the inner portion of the shell starts to decrease, reversing its sign at stagnation. This is a crucial point of the implosion since no more "pdV" compression work can be done to the hot spot after the stagnation, and the only remaining heating source is the energy deposition of α particles produced by fusion reactions inside the hot spot (α heating). At the deceleration phase of the implosion, the kinetic energy of the shell is transferred into the internal energy of the hot spot. To ignite the fuel, the energy gain due to the pdV work of the imploding shell and α heating must be larger than the energy losses due to thermal conduction and radiation. This requirement sets a minimum value for the implosion velocity v_{imp} of the shell.

The following sections review the basic concept of ICF ignition, present the simplest direct-drive ignition target design, and discuss stability issues.

Basic Concepts

To burn a substantial fraction of the fuel mass, the fuel density at stagnation must be very large. This can be easily shown if we assume that the main fuel at the peak compression is assembled as a uniform-density sphere with a radius R_f and density ρ_m.[1,2] The reaction rate is given by $dn/dt = n_D n_T \langle\sigma v\rangle$, where $\langle\sigma v\rangle$ is the average reactivity, n_D and n_T are the density of deuterium and tritium, respectively, and n is the number density of the reacted fuel. Assuming a 50/50 DT mixture, $n_D = n_T = n_0/2 - n$, where n_0 is the initial density. To calculate the total number of reactions, we integrate $N = \int_0^{t_d} V(t)\left(dn/dt\right)dt$ over the burn duration time t_d, where $V(t)$ is the volume of the burning fuel. The burn time is determined by the fuel disassembly rate. Since there is no external force to keep the fuel together after the stagnation, the outer region of the fuel expands, launching a rarefaction wave toward the center. The rarefaction wave propagates at the local sound speed c_s and it takes approximately $t_d = R_f/c_s$ for the whole sphere to decompress and cool down, quenching the fusion reactions. During the decompression, only the high-density portion of the fuel inside the radius $R(t) = R_f - c_s t$ is burning. Since the total number of reactions is proportional to the time integral of the burning fuel volume, we can define an effective confinement time t_c as $\int_0^{t_d} V(t)dt = V_0 t_c$, where $V_0 = 4\pi R_f^3/3$. The integration gives $t_c = t_d/4$. If the number of fused atoms is small, $n \ll n_0$, then the total number of reactions becomes $N = n_0^2\langle\sigma v\rangle V_0 t_c/4$. The ratio $f = N/N_0$ is commonly referred to as a burn fraction, where $N_0 = n_0 V_0/2$

is the initial number of DT pairs. Substituting N into f gives $f = n_0 R_f \langle\sigma v\rangle / 8\, c_s = \rho_m R_f / \left(8\, c_s m_{\rm DT} / \langle\sigma v\rangle\right)$, where $m_{\rm DT}$ is the DT ion mass. The combination $8\, c_s m_{\rm DT} / \langle\sigma v\rangle$ has a minimum value of 6 g/cm^2 at the ignition conditions; to have an efficient burn, the fuel must reach $\rho_m R_f > 1$ g/cm^2 at peak compression (more accurate calculations show that $f = 0.3$ at $\rho_m R_f = 3$ g/cm^2). Using such an estimate, we can determine the maximum density of the assembled fuel and convergence ratio of the shell at ignition. Assuming that a fraction f_H of the laser energy E_L goes into the shell kinetic energy $M v_{\rm imp}^2 / 2$, the shell mass M can be expressed as $M = 2\, f_H E_L / v_{\rm imp}^2$. The fraction f_H is a product of the hydrodynamic efficiency (defined as a ratio of the shell kinetic energy to the absorbed laser energy, typically ~10% for a direct-drive implosion) and the laser absorption fraction of ~0.6. This yields $f_H \sim 0.06$. The fuel mass at stagnation can be rewritten as $M = 4\pi\left(\rho_m R_f\right)^3 / 3\rho^2$. Equating the two expressions for the mass, we obtain the fuel density at the peak compression

$$\rho_m = v_{\rm imp} \sqrt{\frac{2\pi\left(\rho_m R_f\right)^3}{3 f_H E_L}}. \tag{1}$$

The value of $\rho_m R_f \simeq 2$ g/cm^2 is fixed by the fuel burnup fraction. The implosion velocity cannot be much less than 3×10^7 cm/s to have a temperature increase inside the hot spot during the shell deceleration (energy gain exceeds the energy losses at such a velocity). Using these values gives $\rho_m\left(\text{g/cm}^3\right) \simeq 160 / \sqrt{E_L(\text{MJ})}$, where the laser energy is measured in megajoules. For an $E_L = 1$ MJ facility, $\rho_m = 160$ g/cm$^3 \simeq 630\, \rho_{\rm DT}$, where $\rho_{\rm DT} = 0.25$ g/cm^3 is the density of cryogenic uncompressed DT mixture at $T = 18$ K. To find the shell convergence ratio $C_r = R_0 / R_f$ required to achieve such a high density, we write the mass conservation equation $4\pi\rho_{\rm DT} R_0^3 \left(1 - f_A\right) / A_0 = 4\pi\rho_m R_f^3 / 3$, where $A_0 = R_0 / \Delta_0$ is the initial aspect ratio, R_0 and Δ_0 are the inner radius and thickness of the undriven shell, and f_A is the fraction of the shell mass ablated during the implosion. For a typical direct-drive ignition design, $f_A \simeq 0.8$. This leads to

$$C_r \simeq \left(\frac{5}{3} A_0 \frac{\rho_m}{\rho_{\rm DT}}\right)^{1/3}. \tag{2}$$

Taking $A_0 = 4$ and $\rho_m / \rho_{\rm DT} = 630$ gives $C_r = 16$.

So far, we considered only conditions for the high-ρR fuel assembly. To initiate the burn wave inside the main fuel, as mentioned earlier, the hot spot must first reach ignition conditions. Since the reaction rate is proportional to p^2 ($dn/dt \sim n^2 \langle\sigma v\rangle$ and $\langle\sigma v\rangle \sim T^2$ for $T > 6$ keV, this gives $dn/dt \sim p^2$), high pressure must be achieved inside the hot spot. We can estimate the pressure evolution inside the hot spot during the deceleration phase by considering an adiabatic compression of a gas by a spherical piston. The adiabatic condition relates the pressure and density as $p \sim \rho^{5/3}$. Then the mass conservation yields $\rho R^3 = \rho_d R_d^3$ or $\rho \sim R^{-3}$, where ρ_d and R_d are the mass density and radius at the beginning of deceleration. This gives

$$p = p_d \left(\frac{R_d}{R}\right)^5. \tag{3}$$

Strictly speaking, the hot-spot compression cannot be considered as adiabatic during the deceleration phase because of thermal conduction effects. A detailed calculation including thermal conduction losses,[3] however, shows that an R^{-5} law is valid in a more general case (not including α deposition). This can be easily explained if we consider pressure as an internal energy density. The thermal conduction deposits part of the hot-spot energy into heating the inner layer of the surrounding cold shell. The heated layer then ablates and the ablated mass returns the lost energy back into the hot spot. With the help of Eq. (3), we can calculate the shell trajectory during the deceleration using Newton's law;

$$M \frac{d^2 R}{dt^2} = 4\pi p R^2. \tag{4}$$

Integrating the latter equation gives

$$v^2 = v_{\rm imp}^2 + \frac{4\pi p_d R_d^3}{M}\left(1 - C_{rd}^2\right), \tag{5}$$

where $C_{rd} = R_d / R$. At stagnation, $v = 0$ and Eq. (5) yields the total convergence ratio

$$C_{rd} \sim \sqrt{1 + \frac{E_k}{E_i}}, \tag{6}$$

where $E_k = M v_{\rm imp}^2 / 2$ and

$$E_i = \frac{4\pi}{3} \frac{p_d}{(\gamma - 1)} R_d^3 = 2\pi p_d R_d^3$$

is the shell kinetic energy and the total internal energy of the gas at the beginning of the deceleration phase, respectively, and γ is the ratio of specific heats [we used $\gamma = 5/3$ in Eq. (6)]. The relation (6) is satisfied only approximately since it does not take into account the pressure increase due to α deposition. Such an effect is important, however, only near stagnation. Using the limit $E_k \gg E_i$, the maximum pressure takes the form

$$p_m = \frac{1}{p_d^{3/2}}\left(\frac{E_k}{3V_d}\right)^{5/2}, \tag{7}$$

where $V_d = 4\pi R_d^3/3$. Equation (7) shows that to achieve the hot-spot ignition (high pressure) we must minimize, for a given kinetic energy, the gas pressure and radius R_d at the beginning of shell deceleration (when the reflected shock starts interacting with the shell). The next section will explain how such a minimization is achieved in a direct-drive ignition target.

Direct-Drive Ignition Target Design

High density and convergence ratio requirements put a limitation on the maximum entropy increase in the shell during an implosion. Let us assume that the pressure increases from its initial value p_0 inside the shell to the ablation pressure p_a at the maximum laser intensity. The density ρ is at its maximum when the shell entropy increase is zero ($\Delta s = 0$) during the compression (adiabatic implosion); $\rho/\rho_0 = \left(p_a/p_0\right)^{1/\gamma} e^{-\Delta s/c_p}$, where c_p is the specific heat at constant pressure and ρ_0 is the initial density. It is not feasible, however, to drive a perfectly adiabatic implosion. Shock waves, radiation preheat, hot-electron preheat, and others increase the entropy during the shell compression. We can minimize the hydrodynamic part in the entropy change, nevertheless, by accurately timing all hydrodynamic waves launched into the target during the laser drive. The shell entropy is commonly characterized by the adiabat $\alpha = p/p_F$, which is defined as the ratio of the shell pressure p to the Fermi-degenerate pressure (mainly because of electrons) p_F calculated at the shell density. The Fermi pressure of an electron gas has the form $p_F = \mu\rho^{5/3}$, where $\mu = (3\pi^2)^{2/3}\hbar^2 Z^{5/3}/5m_i^{5/3}m$, m and m_i are electron and ion masses, respectively, $\hbar$ is the Planck constant, and Z is the ion charge. For fully ionized DT, $\mu = 2.15\left[\text{Mbar}/\left(\text{g/cm}^3\right)^{5/3}\right]$. Since the shell entropy during an implosion is a crucial parameter, the target design in ICF is characterized by the adiabat value. For example, an "α = 3 design" means that the pressure inside the shell during the implosion in such a design is three times larger than the Fermi-degenerate pressure of the fully ionized DT.

Next we consider the simplest direct-drive target design, which consists of a spherical DT-ice shell filled with DT gas. The main fuel in the shell is kept at cryogenic temperatures (~18 K) to maximize the fuel mass and minimize the shell entropy. The initial shell thickness is Δ_0 and the inner shell radius is $R_0 \gg \Delta_0$. The target is driven by a laser pulse that consists of three distinct regions: a low-intensity foot, a transition region, and the main drive [see Fig. 106.23(a)]. The main parameters of the laser pulse are the foot length t_0, end of the rise time t_r, end of the pulse t_{end}, foot power P_0, and maximum power P_{max}. During the foot, a shock wave (SW1) launched at the beginning of the pulse propagates through the shell. The adiabat of the post-shock material depends on the shock strength, which, in turn, is a function of the laser intensity. Thus, the foot power P_0 is chosen to set the post-shock material on a desired adiabat α. Analytical models[1,4] predict that the drive pressure and the laser intensity I are related as $p(\text{Mbar}) = 40\left(I_{15}/\lambda_L\right)^{2/3}$, where I_{15} is measured in 10^{15} W/cm^2 and λ_L is the laser wavelength measured in

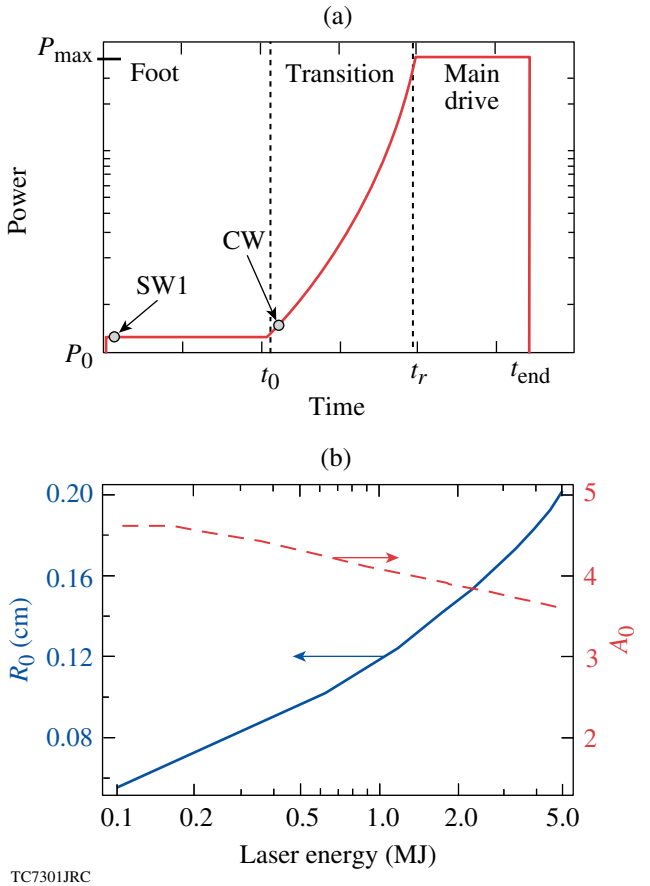

Figure 106.23
(a) Laser drive pulse for a direct-drive target. (b) The dimensions of direct-drive ignition targets versus laser energy ($v_{\text{imp}} = 4.5 \times 10^7$ cm/s).

microns. Substituting $p = \alpha\mu\rho_1^{5/3}$ into the latter equation shows that the laser intensity scales with α in a DT shell driven by a $\lambda_L = 0.351$ μm laser as $I_{12} = 4\alpha^{3/2}$, where the intensity is measured in TW/cm^2 and the post-shock density is $\rho_1 \simeq 4\rho_{\mathrm{DT}} =$ 1 g/cm^3 in the strong-shock limit. The 3/2 power law does not take into account an intensity dependence in the laser absorption. When the latter is included (with the help of numerical simulations), the required laser intensity becomes $I_{12} = 7\alpha^{5/4}$. Using this result, we obtain a relation between the foot power and the shell adiabat; $p_0(\mathrm{TW}) = 90\, R_0^2\left(1 + 1/A_0\right)^2\alpha^{5/4}$. Next, as the laser intensity increases during the transition time, a compression wave (CW) is launched into the shell. To prevent an adiabat increase, such a wave should not turn into a strong shock inside the shell. This determines the intensity slope in the transition region. To maintain an adiabatic compression during the rise time, one can use Kidder's solution[5] for the drive pressure. This gives the power history during the transition time

$$P = \frac{\hat{P}}{\left[1 - \left(t/T_c\right)^2\right]^{\omega}}, \tag{8}$$

where T_c and $\hat{P}$ are normalization coefficients determined from matching P with P_0 at $t = t_0$ and $P = P_{\max}$ at $t = t_r$. Numerical simulations show that moderate variations in ω $(2 < \omega < 7)$ do not significantly affect the shell adiabat. Since there are limitations on the maximum power imposed by both instabilities because of the laser–plasma interaction and damage threshold issues, the laser power cannot follow Eq. (8) at all times. Thus, we assume that the laser power becomes flat after time t_r when P reaches the peak power $P_{\max}$ [see Fig. 106.23(a)].

Next, we consider what determines the values of t_0 and t_r. The CW, as any linear sound wave in hydrodynamics, travels with the local sound speed and eventually catches up with the SW1. After coalescence, both the shock strength and the adiabat of the post-shock material increase. Minimizing the shell adiabat, we must prevent the CW and SW1 coalescence inside the shell. This sets the minimum value of t_0. Conversely, if t_0 is too large, the SW1 and CW will be well separated in time. As the SW1 breaks out at the shell's rear surface, the surface starts to expand, launching a rarefaction wave (RW) toward the ablation front. The RW establishes some velocity, pressure, and density gradients in its tail. Since the CW and RW travel in opposite directions, they meet inside the shell. At this instant, the CW starts to propagate along the hydrodynamic gradients established by the RW. It is well known in hydrodynamics that a sound wave traveling along a decreasing density turns into a shock sooner than a sound wave traveling through a uniform or increasing density. As the CW turns into a shock, the latter will excessively increase the shell entropy, reducing the shell convergence ratio. The foot duration t_0 can be related to the shell adiabat α and the initial shell thickness Δ_0. Using Hugoniot jump conditions across the shock, one can easily obtain the shock velocity; neglecting spherical convergence effects, $U_s(p_1 \gg p_0) = \sqrt{(\gamma + 1)p_1/2\rho_0}$, where p_0 and p_1 are the initial and post-shock pressure, respectively. The SW1 transit time through the shell becomes $t_{\mathrm{sh}} = \Delta_0/U_s$. The CW travels through the shock-compressed shell with a thickness $\Delta_c = \Delta_0\rho_0/\rho_1$, where ρ_0 and ρ_1 are the initial and post-shock density, respectively. The CW propagation time is $t_{\mathrm{cw}} = \Delta_c/c_1$, where $c_1 = \sqrt{\gamma p_1/\rho_1}$. Thus, the foot length takes the form $t_0 = t_{\mathrm{sh}} - t_{\mathrm{cw}}$. Using expressions for the shock velocity and the adiabat yields the following equations for t_0 and t_{sh}:

$$t_0(\mathrm{ns}) = 0.016\frac{\Delta_0(\mu\mathrm{m})}{\sqrt{\alpha}}$$

and (9)

$$t_{\mathrm{sh}}(\mathrm{ns}) = 0.03\frac{\Delta_0(\mu\mathrm{m})}{\sqrt{\alpha}},$$

where $\gamma = 5/3$. Similar to t_0, the rise time t_r is also determined by avoiding an additional strong-shock formation. The transition region cannot be too short; the CW otherwise turns into a shock. The time t_r also cannot be too large. This is due to the formation of a second shock wave (SW2) inside the shell. It is easy to show that an adjustment wave (AW) is formed as the leading edge of the RW breaks out at the ablation front. Each fluid element inside the RW is accelerated according to $\mathrm{d}v/\mathrm{d}t = -\partial_x p/\rho$. At the head of the RW, ρ is equal to the shell density compressed by the SW1 and CW. When the leading edge reaches the ablation front, the density suddenly drops, creating a large gradient in the acceleration of fluid elements. This forms a local excess in the pressure that starts to propagate in the form of a compression (adjustment) wave along a decreasing density profile of the RW tail. As mentioned earlier, the AW traveling along a decreasing density turns into a shock inside the shell.[6] Thus the SW2 is formed even for a constant-intensity laser pulse.

The formation of the AW can also be shown by comparing the following density profiles: In the first case, the profile is created by a rarefaction wave traveling across a uniform-density foil. For the second profile, we take a solution of the motion equation for an accelerated foil. The solution for a rarefaction wave profile can be found using a self-similar analysis.[7] Calculated at the breakout time of the leading edge, the density becomes

$$\rho = \rho_{a1}\left(\frac{\bar{x} + d_1}{d_1}\right)^3, \tag{10}$$

where $\bar{x}$ is the position in the frame of reference moving with the ablation front ($\bar{x} = 0$ at the ablation front), $\gamma = 5/3$, and d_1 is defined as $\rho(-d_1) = 0$. Conversely, during the shell acceleration, the density profile can be found by solving Newton's equation

$$\rho g = \frac{\partial p}{\partial x}. \tag{11}$$

Assuming that the entropy is uniform across the entire shell, the pressure is related to the density as $p = \mu\alpha\rho^{5/3}$, and the solution of Eq. (11) takes the form

$$p = p_a\left(1 + \frac{\bar{x}}{d_2}\right)^{5/2}, \tag{12}$$

where $d_2 = 5\mu^{3/5}\alpha^{3/5}p_a^{2/5}\big/2g$. Then, the adiabatic relation $\rho = (p/\mu\alpha)^{3/5}$ gives

$$\rho = \rho_{a2}\left(\frac{\bar{x} + d_2}{d_2}\right)^{3/2}. \tag{13}$$

The comparison of Eqs. (10) and (13), keeping the same mass for the two profiles, gives the relation between the shell thicknesses

$$d_2 = \frac{5}{8}\left(\frac{p_{a1}}{p_{a2}}\right)^{3/5} d_1. \tag{14}$$

Since $p_{a1} \le p_{a2}$ (the shell is accelerated during the main pulse where the intensity reaches the maximum value), we conclude that the shell during the acceleration should be more compact than that produced by a rarefaction wave; $d_2 < d_1$. This is possible only if a compression wave is launched into the shell at the beginning of the acceleration.

Even though the SW2 cannot be avoided, its strength and effect on target performance can be minimized by appropriately choosing t_r. An intensity rise prior to the leading edge of the RW breakout at the ablation front helps to steepen the density profile, reducing the AW strength. If t_r is too large and the SW2 formation occurs during the drive-pressure rise, the SW2 will be too strong, raising the pressure in the vapor. Thus, t_r must be between the SW1 breakout at the rear surface and the leading edge of the RW breakout at the ablation front (in other words, the laser must reach the peak power while the leading edge of RW is inside the shell). This concludes the pulse-shape specification for a simple direct-drive ignition design.

Next, we determine the optimum target radius R_0 and shell thickness Δ_0 for a given laser energy. The following effects must be considered: After the SW1 breaks out at the back of the shell, a transmitted shock is formed in the vapor. This shock reaches the center, reflects, and eventually interacts with the incoming shell. During the reflected-shock propagation through the shell, the shell decelerates (deceleration phase of an implosion). If R_0 is too large, the laser is turned off well before the beginning of the deceleration phase. The shell then coasts inward between the end of the drive pulse and beginning of deceleration. Both the front and back surfaces of the shell expand, in the frame of reference moving with the main fuel, during the coasting phase, reducing the shell density. To maximize the density, the duration of the coasting phase must be minimized. This sets an upper limit on R_0. In the opposite case, when R_0 is too small, the reflected shock interacts with the shell while the laser pulse is still on. The pressure inside the shell in this case increases above the drive-pressure value and the shell acceleration therefore goes to zero, preventing an effective transfer of the laser absorbed energy into the kinetic energy of the shell. Thus, the end of the pulse in an optimized design should occur after the main shock reflection from the target center, but before the beginning of the deceleration phase.

Accounting for the optimization arguments listed earlier, we plot the shell radius and initial aspect ratio $A_0 = R_0/\Delta_0$ versus the incident laser energy in Fig. 106.23(b), keeping the maximum laser intensity at $I_{\max} = 10^{15}$ W/cm^2 and the implosion velocity at $v_{\text{imp}} = 4.5 \times 10^7$ cm/s. Calculations show that the target dimensions do not have a strong dependence on the shell adiabat. The shell radius is fitted well with a 1/3-power law $R_0 = 0.06\left[E_L(\text{MJ})/0.1\right]^{1/3}$. The shell thickness, on the other hand, has a stronger energy dependence; $\Delta_0 = 0.012\left[E_L(\text{MJ})/0.1\right]^{1/2.6}$. A deviation from the $E_L^{1/3}$ scaling in Δ_0 (which is expected from a simple $E_L \sim D^3$ argument, where D is a scale length of the problem) is due to a scale-length dependence in the laser absorption (the smaller the target, the steeper the density scale length, and, therefore, the smaller absorption fraction). This results in an increased initial aspect ratio for the lower laser energies, as shown in Fig. 106.23(b).

Using the obtained target dimensions and laser pulse shapes, the gain curves and the maximum shell ρR can be calculated with a one-dimensional hydrocode. These are shown in Fig. 106.24. Figure 106.24(a) indicates that the designs with the

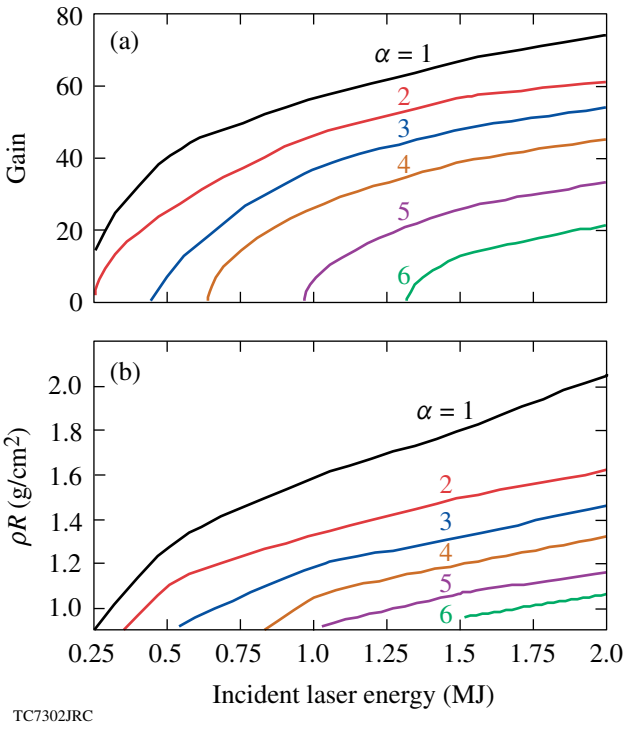

Figure 106.24
(a) Gain curves and (b) maximum ρR for ignition direct-drive targets.

shell adiabat up to $\alpha = 6$ are expected to ignite on the National Ignition Facility with the incident laser energy $E_L = 1.5$ MJ.

Stability

Hydrodynamic instabilities put severe constraints on target designs because they limit the maximum convergence ratio and temperature of the hot spot.[1,8] The dominant hydrodynamic instability in an ICF implosion is the Rayleigh–Taylor (RT) instability. The RT instability inevitably occurs in systems where the heavier fluid is accelerated by the lighter fluid.[9] Such conditions arise during the shell compression in ICF implosions where the heavier shell material is accelerated by the lighter blowoff plasma. The RT instability growth amplifies the shell distortions seeded by initial surface roughness and laser nonuniformities (laser "imprint"). If allowed to grow to substantial amplitudes, the shell nonuniformities reduce the shell ρR and the neutron yield. Fortunately for ICF implosions, the thermal conduction that drives the ablation process creates several stabilizing effects that reduce both the nonuniformity seeding and the RT growth rates.[10,11] Seeding due to the laser nonuniformity is determined by how quickly the plasma atmosphere is created around the imploding shell. The laser irradiation is absorbed at some distance from the cold shell. The larger this distance (the conduction zone), the larger the smoothing effect of the thermal conductivity within the conduction zone and the smaller the laser imprint. The RT modes are also stabilized by the thermal conductivity that drives the mass ablation of the shell material. The ablation process is characterized by the ablation velocity V_a, which is defined as the ratio of the mass ablation rate to the shell density $V_a = \dot{m}/\rho_{\mathrm{sh}}$. The larger the value of the ablation velocity, the larger the ablative stabilization. Taking thermal smoothing and ablative stabilization into account, one can make a general statement that the higher the initial intensity of the drive laser pulse (larger P_0), the smaller the nonuniformities and the more stable the implosion. Indeed, the higher intensity tends to create the conduction zone in a shorter time, reducing the laser imprint. In addition, the initial shock launched by the higher-intensity pulse is stronger, resulting in higher shell adiabat. This reduces the shell density, increasing the ablation velocity. Furthermore, a lower density leads to an increase in the shell thickness and a reduction in the perturbation feedthrough from the ablation front to the shell's rear surface (which becomes unstable during the deceleration phase of the implosion). There is a price to pay, however, for the greater stability. As the stronger shock propagates through the shell, it places the shell material on a higher adiabat. This leads to a reduction in target gain and shell ρR, as shown in Fig. 106.24. A common practice in designing direct-drive targets is to find the delicate balance between a reduction in the target performance due to an increase in the adiabat and the increase in shell stability.

In optimizing the target design, one can take into consideration that the RT modes are surface modes peaked at the ablation surface of the shell. To reduce the instability growth, it is therefore sufficient to raise the adiabat only at the outer region of the shell, which ablates during the implosion. If the inner portion of the shell is kept on a lower adiabat, the shell and vapor compressibility will not be reduced during the final stage of implosion and the neutron yields will be unaffected by this selective adiabat increase (adiabat shaping). The shell adiabat is shaped by launching a shock, whose strength decreases as it propagates through the shell.[12] This places an adiabat gradient directed toward the ablation front. A time variation in the shock strength is imposed by replacing the foot with an intensity picket in front of the main-drive pulse. The picket launches a strong shock that propagates through the shell. As the laser intensity drops at the end of the picket, the shocked material starts to expand and a rarefaction wave is launched toward the shock. After the rarefaction and the shock coalesce, the shock strength decays, reducing the adiabat of the shock-compressed material. Implementing the adiabat shaping to the direct-drive ignition target designs shows a significant improvement in shell

stability without compromising the target gain. This is illustrated in Fig. 106.25, where two target designs with (a) a foot and (b) an intensity picket in front of the main drive are shown at the end of the acceleration phase. The isodensity contours are obtained using the two-dimensional hydrocode *ORCHID*.[13] An improvement in the shell stability increases our confidence in the success of the direct-drive ignition campaign on NIF.

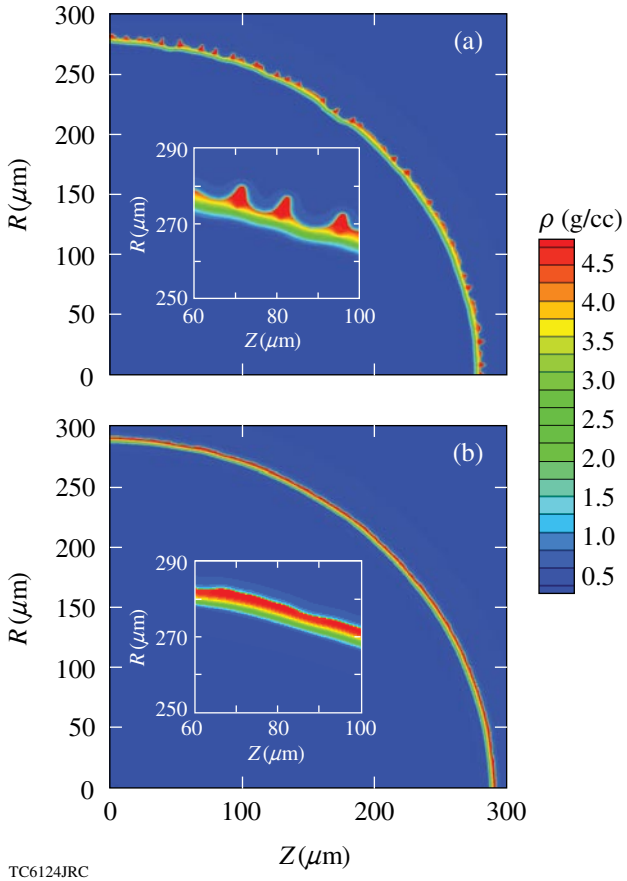

Figure 106.25
Isodensity contours of the (a) standard and (b) picket OMEGA $\alpha = 3$ target designs.

ACKNOWLEDGMENT

This work was supported by the U.S. Department of Energy Office of Inertial Confinement Fusion under Cooperative Agreement No. DE-FC52-92SF19460, the University of Rochester, and the New York State Energy Research and Development Authority. The support of DOE does not constitute an endorsement by DOE of the views expressed in this article.

REFERENCES

1. J. D. Lindl, *Inertial Confinement Fusion: The Quest for Ignition and Energy Gain Using Indirect Drive* (Springer-Verlag, New York, 1998).
2. M. D. Rosen, Phys. Plasmas **6**, 1690 (1999).
3. R. Betti, K. Anderson, V. N. Goncharov, R. L. McCrory, D. D. Meyerhofer, S. Skupsky, and R. P. J. Town, Phys. Plasmas **9**, 2277 (2002).
4. W. M. Manheimer, D. G. Colombant, and J. H. Gardner, Phys. Fluids **25**, 1644 (1982).
5. R. E. Kidder, Nucl. Fusion **14**, 53 (1974).
6. R. Betti, V. Lobatchev, and R. L. McCrory, Phys. Rev. Lett. **81**, 5560 (1998).
7. L. D. Landau and E. M. Lifshitz, *Fluid Mechanics*, 2nd ed., Course of Theoretical Physics, Vol. 6 (Butterworth-Heinemann, Newton, MA, 1987).
8. S. Atzeni and J. Meyer-ter-Vehn, *The Physics of Inertial Fusion: Beam Plasma Interaction, Hydrodynamics, Hot Dense Matter*, International Series of Monographs on Physics (Clarendon Press, Oxford, 2004).
9. S. Chandrasekhar, in *Hydrodynamic and Hydromagnetic Stability*, International Series of Monographs on Physics (Clarendon Press, Oxford, 1961).
10. J. Sanz, Phys. Rev. Lett. **73**, 2700 (1994).
11. V. N. Goncharov, R. Betti, R. L. McCrory, P. Sorotokin, and C. P. Verdon, Phys. Plasmas **3**, 1402 (1996).
12. V. N. Goncharov, J. P. Knauer, P. W. McKenty, P. B. Radha, T. C. Sangster, S. Skupsky, R. Betti, R. L. McCrory, and D. D. Meyerhofer, Phys. Plasmas **10**, 1906 (2003).
13. R. L. McCrory and C. P. Verdon, in *Computer Applications in Plasma Science and Engineering*, edited by A. T. Drobot (Springer-Verlag, New York, 1991).